AGU PUBLICATIONS

JGR

Journal of Geophysical Research: Space Physics

RESEARCH ARTICLE
10.1002/2014JA020842

Special Section:
Low-Frequency Waves in Space Plasmas

Key Points:
- Equatorward drift of presubstorm auroras
- Ionospheric currents associated with equatorward drift of auroras
- Ionospheric currents generate high-m ULF waves in the magnetosphere

Supporting Information:
- Readme
- Animation S1

Correspondence to:
O. Saka,
saka.o@nifty.com

Citation:
Saka, O., K. Hayashi, and A. S. Leonovich (2015), Ionospheric loop currents and associated ULF oscillations at geosynchronous altitudes during preonset intervals of substorm aurora, *J. Geophys. Res. Space Physics, 120*, doi:10.1002/2014JA020842.

Received 17 NOV 2014
Accepted 26 FEB 2015
Accepted article online 28 FEB 2015

Ionospheric loop currents and associated ULF oscillations at geosynchronous altitudes during preonset intervals of substorm aurora

O. Saka[1], K. Hayashi[2], and A. S. Leonovich[3]

[1]Office Geophysik, Ogoori, Japan, [2]Earth and Planetary Physics, University of Tokyo, Tokyo, Japan, [3]Institute of Solar-Terrestrial Physics, Siberian Branch of Russian Academy of Sciences, Irkutsk, Russia

Abstract A substorm aurora was observed at 04:52 UT on 27 January 1986 by an all-sky imager installed at Shamattawa (66.3°N, 336.0° in corrected geomagnetic coordinates) and a magnetometer on board a conjugate satellite (GOES 6) at geosynchronous altitudes. In the preonset intervals lasting for approximately 50 min prior to the expansion onset, an equatorward drift of the auroras beginning from 71°N to 64°N was observed. Meanwhile, GOES 6 observed ULF oscillations in 25–200 s periods at geosynchronous altitudes after about 10 min following the start of the equatorward drift. During the equatorward drift of the arc, the flow reversal occurred, where the auroral arc propagating eastward was replaced by a westward propagation. Simultaneously, the major axes of the ULF oscillations rotated clockwise by ~90° in the equatorial plane. We conclude that the ULF oscillations are azimuthally small-scale Alfvén waves excited in the magnetosphere by field-aligned currents associated with ionospheric loop currents.

1. Introduction

Standing Alfvén waves with an azimuthal wavelength much smaller than that along field lines are often referred to as high-*m* waves, where *m* is the azimuthal wave number. These waves can be excited by the currents in the ionosphere [*Leonovich and Mazur*, 1993] or magnetosphere [*Mager and Klimushkin*, 2008] and amplified by high-energy particles either through drift bounce resonance [*Karpman et al.*, 1977; *Glassmeier et al.*, 1999] or by MHD instabilities of the Geotail current sheet [*Hameiri et al.*, 1991; *Klimushkin et al.*, 2012].

High-*m* waves originate at the poloidal surface and propagate across the magnetic shell to the toroidal surface [*Leonovich and Mazur*, 1993]. The poloidal surface is where wave frequency matches the poloidal Alfvén wave eigenfrequency, and toroidal surface is where it matches the toroidal Alfvén wave eigenfrequency. The difference between the eigenfrequencies of poloidal and toroidal surfaces is referred to as the polarization splitting of the Alfvén oscillations [*Leonovich and Mazur*, 1990].

The poloidal polarizations of the Alfvén waves generated in the magnetosphere are converted to its toroidal polarization in the process of wave travel to the toroidal surface, where the wave terminates [*Leonovich and Mazur*, 1993]. Depending on the relative position of the resonant surfaces, these waves can be propagated in either a poleward or equatorward direction when projected to the ionosphere. If plasmas in much of a field line are "cold" ($\beta \ll 1$, where $\beta = 8\pi P/B^2$ is the ratio of the gas-kinetic plasma pressure to the magnetic pressure), the toroidal resonance shell is nearer the pole of the poloidal shell. In this case, the waves propagate poleward [*Leonovich and Mazur*, 1993]. By contrast, if β~1, the toroidal shell can be nearer the equator of the poloidal shell, and these waves then propagate equatorward [*Kozlov et al.*, 2006]. The first scenario is most probable under quiet geomagnetic conditions, when the plasma is cold on the bulk of the field line. The second likely occurs in presubstorm conditions, when the cold plasma is replaced by a "warm" plasma on the bulk of field line.

The equatorward drift of the auroral arc contained azimuthal drifts in the east-west directions with velocities faster than those in the equatorward drift [*de la Beaujardiere et al.*, 1994; *Saka et al.*, 2014], which resulted in a tilted arc from the geomagnetic east-west lines. The group of these arcs formed the wavefront of the high-*m* Alfvén waves propagating equatorward periodically, where *m* denotes the wave number encircling the Earth [*Saka et al.*, 2014]. In this report, we examine the equatorward drift of the auroral arc in an all-sky imager in conjunction with the magnetometer data from the conjugate satellite at the geosynchronous orbit.

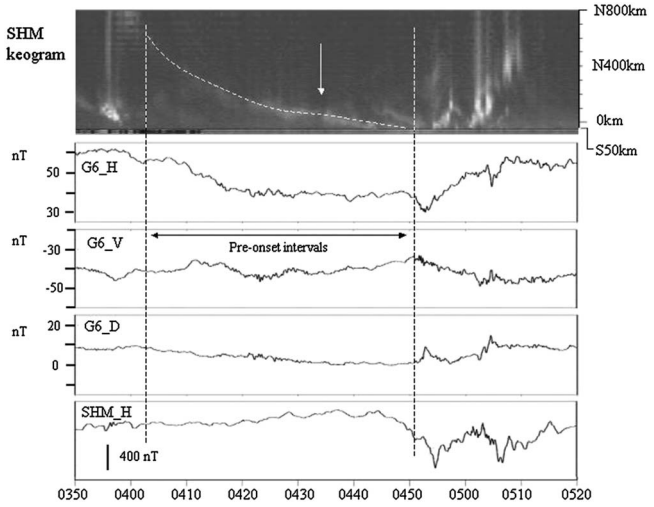

Figure 1. (top to bottom) A 1 h 30 min plot from 03:50 UT to 05:20 UT for 27 January 1986, showing a keogram along the geomagnetic meridian crossing SHM from 50 km south to 800 km north of SHM, with the *H*, *V*, and *D* components in the dipole coordinates in nanotesla from the GOES 6 satellite at geosynchronous altitudes. Equatorward expansion of the auroral arc started from 600 km north of SHM at 04:03 UT. It continued until 04:51 UT, when the bead-like rippling was activated at the onset latitudes, 64°N or 200 km south of SHM (see Animation S1 in the supporting information). The time intervals from 04:03 UT to 04:51 UT are denoted as the preonset intervals. The equatorward drift of the preonset auroras is followed by the dotted lines. The vertical arrow marks the gap of the auroral arc (04:34 UT) observed during the equatorward drift.

We show that the high-*m* Alfvén waves are observed by the satellite magnetometer in association with reversals in the azimuthal drift of the arc.

2. Observation

2.1. Magnetometer Observation at Geosynchronous Altitudes

The all-sky imager installed at SHM (Shamattawa; 66.3°N, 336.0° in corrected geomagnetic coordinates) and the magnetometer on board GOES 6 recorded the auroral image and geomagnetic fields at geosynchronous altitudes for auroral substorms occurring on 27 January 1986 in central Canada, respectively. The footprint of the GOES 6 (57.2°N, 260.6° in geographic coordinates), calculated by the IGRF (International Geomagnetic Reference Field) model, was within the field of view of the all-sky imager. Figure 1 shows, from top to bottom, an auroral keogram, *H*, *V*, and *D* component of GOES 6 magnetometer data, and the *H* component of the ground optical station, SHM, from 03:50 UT to 05:20 UT. Satellite signals are plotted using the HVD dipole coordinates, where *H* is positive north parallel to dipole axis, *V* is radial outward, and *D* is dipole east. The substorm started at 04:51 UT, which accompanied decrease of the *H*, decrease of the *V*, and increase of the *D*. The decrease of the ground *H* component, which began at about 04:44 UT, became steeper. These changes occurred in association with the development of bead-like rippling at the onset latitudes prior to the expansions (04:53 UT). The initial activation of the auroras occurred at the poleward boundary at 04:00 UT in a range of 600–800 km north of SHM (72–73°N). Following the poleward activation, the auroras began drifting equatorward toward the onset latitudes (64°N) at an average velocity of ~0.2 km/s, but the drift velocity decreased as it approached the onset latitudes. Note that the keogram did not cover the field of view below 50 km south of SHM because masking tape blocked the moonlight. The auroras at the onset latitudes, however, can be seen in Animation S1 in the supporting information at the equatorward border of the auroras. The interval of the equatorward drift of the aurora from 04:03 UT to 04:51 UT is denoted as the preonset interval marked by the horizontal arrow in Figure 1. ULF oscillations were observed from 04:15 UT to 04:35 UT in all of the three components, *H*, *V*, and *D*. In the keogram, there appeared a

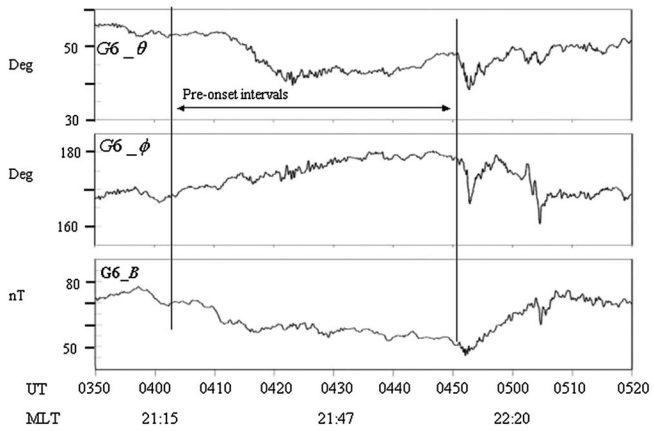

Figure 2. Magnetometer data of GOES 6 converted from the HDV coordinates to the polar coordinated, $B\theta\varphi$ (see text), for the same intervals from 03:50 UT to 05:20 UT. Magnetic local time of the SHM at 04:00 UT, 04:30 UT, and at 05:00 UT is also plotted in the horizontal axis.

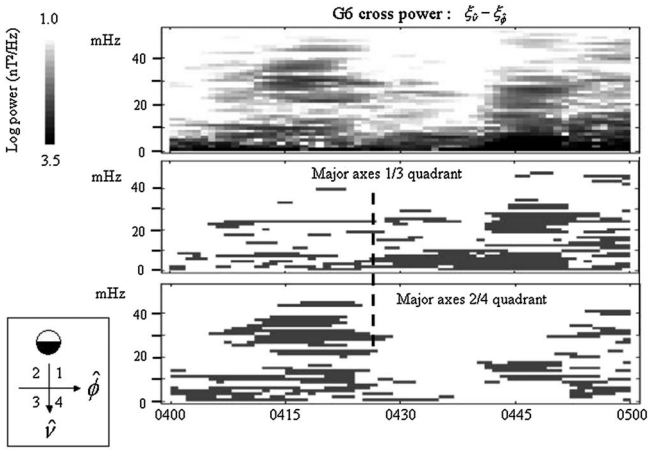

Figure 3. Cross-spectral analyses of the plasma displacement, radial outward ($\hat{v}$), and eastward ($\hat{\phi}$) in the equatorial plane using the FFT method (256 data points of 3 s sampled data). The coordinates used for the plasma displacement are shown in the bottom left corner. The 256 data interval was shifted by 1 min to calculate dynamic spectra. (top) Spectral powers (nT^2/Hz) in 1.0 to 3.5 in logarithmic scale. (middle and bottom) Those spectral bins above 1.5 (nT^2/Hz) were plotted for the orientation angle (see text).

narrow gap, denoted by the vertical arrow at 04:34 UT.

The ULF oscillations observed by GOES 6 at off-equatorial latitudes, 8.8°N in dipole latitudes, can be related to plasma displacement at the equatorial plane by using the polar coordinates of the field line vectors in (B, θ, ϕ), where B is the field magnitude, θ is the inclination angle in degrees measured positive northward from the *V-D* plane, and ϕ represents the azimuth angle of field vectors in degrees in the *V-D* plane measured positive counterclockwise from the *V* axis [*Saka et al.*, 2007, 2010]. The azimuthal angle ϕ is 180° when the field line vectors point earthward. The geomagnetic fields in the HVD coordinates in Figure 1 are converted to the $B\theta\phi$ coordinates in Figure 2. The ULF activities in the preonset interval were observed during the decreasing intervals of the inclination angle, from 55° to 40°. Further decrease of the inclination angle began at 04:51 UT, 2 min prior to the substorm onset characterized by the increase of the inclination angle (dipolarization). The ULF activities are discerned in the transverse plane ($\theta - \phi$) normal to the local field lines.

In the polar coordinates, the transverse perturbations in the meridian plane, $B \cdot \delta\theta\,(b_\theta)$, and those in the azimuthal plane, $B \cdot \delta\phi\,(b_\phi)$, may be related to the plasma displacements in the equatorial plane as

$$\frac{b_\theta}{b_\varphi} = \sin\Theta_0 \frac{\xi_{\hat{v}}}{\xi_{\hat{\phi}}}. \tag{1}$$

Here $\xi_{\hat{v}}$ and $\xi_{\hat{\phi}}$ denote plasma displacement in the equatorial plane in $\hat{v}$ (outward) and in $\hat{\phi}$ (east) components, respectively, used in the dipole field model [*Radoski*, 1974]. The angle Θ_0 denotes inclination of the background field lines. For the preonset intervals, the inclination angles were 45° (Figure 2, top). We can approximate equation (1) using the additional approximation $b_\theta \sim B\delta\theta, b_\phi \sim B\delta\phi$ as

$$\frac{\delta\theta}{\delta\varphi} \sim \frac{\xi_{\hat{v}}}{\xi_{\hat{\phi}}}. \tag{2}$$

Equation (2) suggests that the polarization ellipses in the transverse plane were directly related to the plasma flows in the equatorial plane.

Figure 3 presents the cross-spectral analyses of the plasma displacement in $\hat{v}$ (outward) and in $\hat{\phi}$ (east) components calculated by the fast Fourier transform (FFT) method (256 data points of 3 s sampling data). Figure 3 (top) shows the cross power spectra, and Figure 3 (middle and bottom) are for the orientation of the major axis in the equatorial plane. The orientations are not presented in degrees but are subdivided into four quadrants from 1 to 4 as is shown in the bottom left corner of Figure 3. Spectral bins (12.8 min, shifted by 1 min) above the threshold power were first selected. These bins with major axes in the 1/3 quadrant (rotated clockwise from the radial outward, viewed from above the equatorial plane) are plotted in Figure 3 (middle), while these in the 2/4 quadrants (rotated counterclockwise) are in Figure 3 (bottom). The amplitude resolution of the GOES 6 magnetometer is 0.2 nT, which may correspond to the angular resolutions of 0.2° for the background magnetic fields of 60 nT. To avoid contaminations from low signal levels below the amplitude resolution of the GOES 6 magnetometer, spectral bins with log power level above 1.5 (nT^2/Hz) were selected to plot the major axis. In the preonset interval, ULF oscillations were observed in the two frequency bands: 20–40 mHz and 5–10 mHz. Although the lower-frequency band continued throughout the

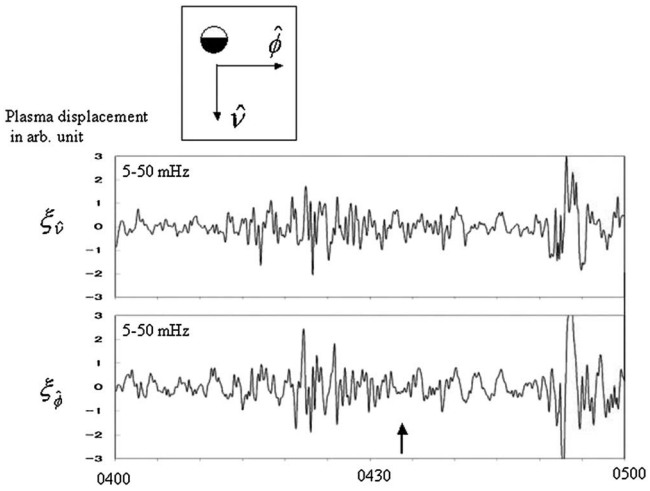

Figure 4. Plots of two components of the plasma displacements in a 5–50 mHz band for the interval from 04:00 UT to 05:00 UT. Oscillations after 04:50 UT are associated with the Pi2 pulsations. The coordinate system shown in the inset at the top is the same as in Figure 3. The amplitudes are expressed in arbitrary unit.

preonset intervals, the higher-frequency band decreased the amplitude level in the second half intervals, as divided by the dotted line. For both frequency bands, however, major axis orientations in 2/4 quadrants switched to the 1/3 quadrants in the second half. The time resolution of the spectral analyses (12.8 min) is not directly comparable to the gap in the keogram, which occurred within 1 min. For a close comparison to the auroras, the band-passed data from 5 mHz to 50 mHz are plotted in Figure 4. The arrow in Figure 4 (bottom) denotes the occurrence time of the gap shown in the keogram. Figure 4 shows that the ULF oscillations in the higher-frequency band decreased in time consistent with the spectral analyses.

The polarization ellipses of the plasma displacement are plotted using hodograms (embedded panels given every 2 min) in Figure 5 from 04:16 UT to 04:50 UT. The major axis in the 2/4 quadrants was replaced by the 1/3 quadrants after 04:34 UT. The rotation of the major axis correlated with the gap in

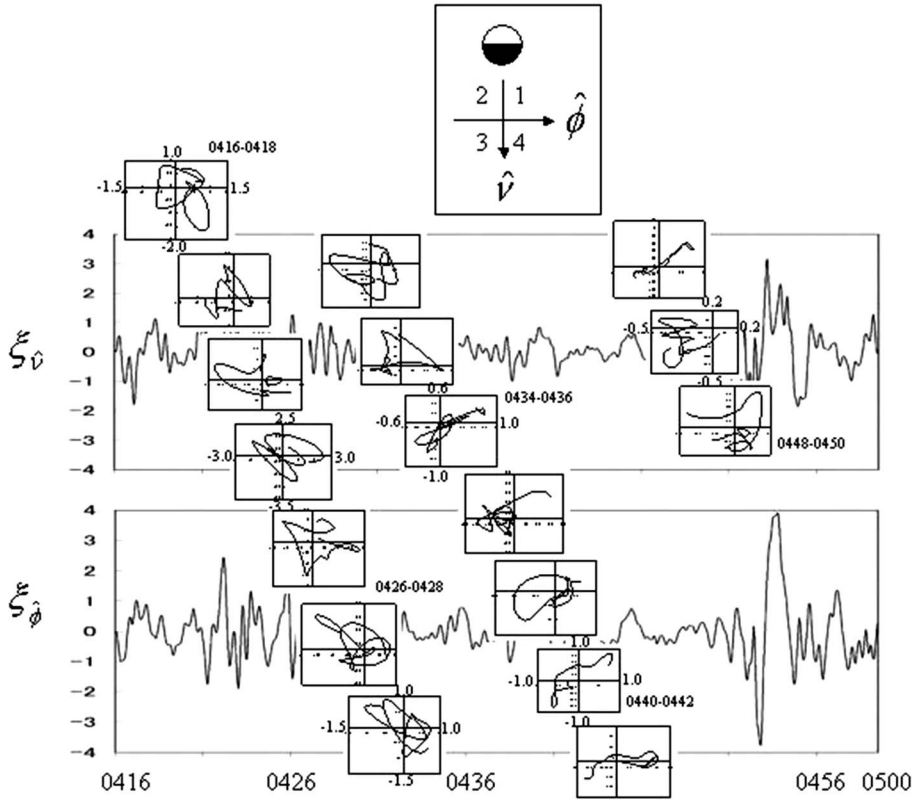

Figure 5. Plots of two components of the plasma displacements on the equatorial plane from 04:16 UT to 04:50 UT. Polarization hodograms in a 5–50 mHz band obtained every 2 min are overlaid from 04:16 UT to 05:04 UT. The rotation of the major axis occurred in the tenth panel designated as 04:34–04:36 UT, without changing the rotation of the ellipses (counterclockwise). This figure is available in colour online at wileyonlinelibrary.com/journal/jgra

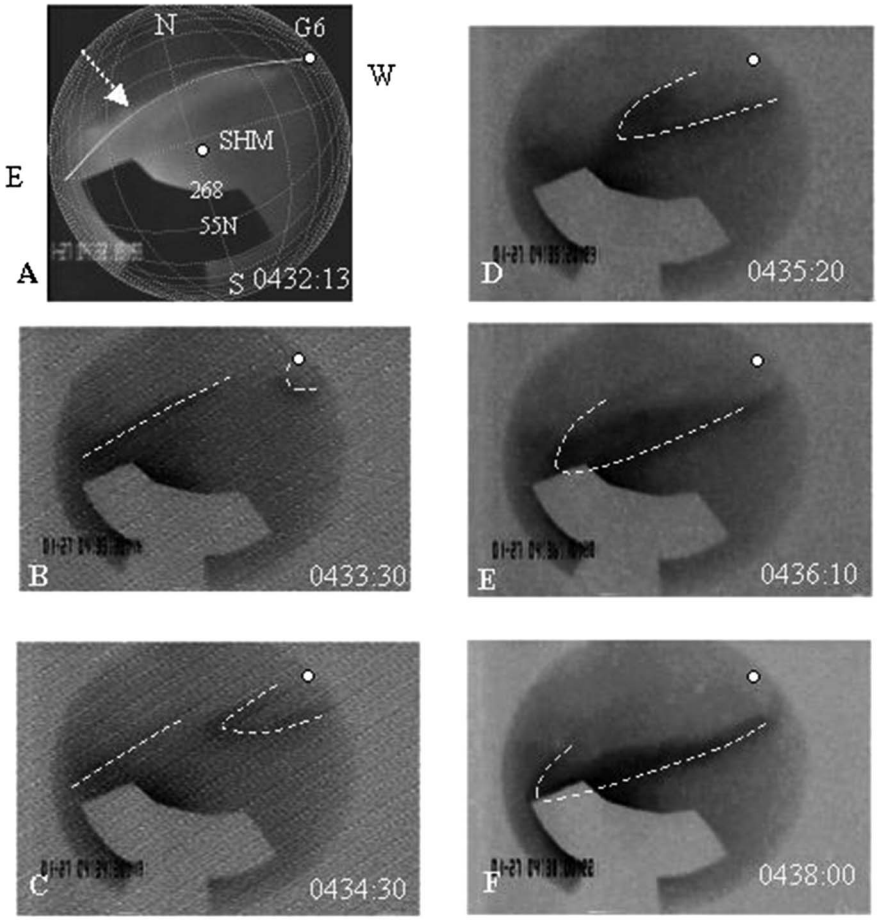

Figure 6. (a–f) Six all-sky images from 04:32:13 UT to 04:38:00 UT for 27 January 1986. Geographic latitudes and longitudes are overlaid in Figure 6a (04:32:13 UT) using grids. Latitudes are plotted every 1°, while the longitudes are for every 2°. The satellite footprints calculated by the IGRF (International Geomagnetic Reference Field) model and a geomagnetic east-west line passing 80 km north of the SHM are also overlaid. The satellite footprints are also plotted in Figures 6b–6f. The magnetometer station, SHM, is at the center of the image. The brighter part of the auroras is in white. West is to the right, east to the left, north is up, and south is down, viewed antiparallel to the field lines. The gray level is reversed in Figures 6b–6f (darker colors for brighter auroras). The sequence sampled at ~10 s from 04:30:00 to 04:55:00 UT is given in Animation S1 in the supporting information. Note that the brighter auroras are in white in the animation. The images in the animation were viewed antiparallel to the field lines in the same manner as the all-sky images in Figure 4. The dark (white in Figures 6e and 6f) portion at the bottom is the masking to block the moonlight.

the aurora by an order of minutes. The orientation switch did not affect the rotation of the polarization ellipses (counterclockwise).

2.2. Auroral Observation

The rotation of the major axis can be seen in the panel labeled "04:34–04:36" UT in Figure 5, which correlates with the gap in the keogram shown by the vertical arrow in Figure 1. All-sky images taken in this gap are presented in Figure 6. These were taken at (Figure 6a) 04:32:13 UT, (Figure 6b) 04:33:30 UT, (Figure 6c) 04:34:30 UT, (Figure 6d) 04:35:20 UT, (Figure 6e) 04:36:10 UT, and (Figure 6f) 04:38:00 UT. The brighter part of the auroras is in white in Figure 6a. For the remaining images (Figures 6b–6f), the brighter part of the auroras is shown in darker colors. The dotted arrow in Figure 6a denotes the auroral arc rotating counterclockwise from the geomagnetic east-west line. The tilt of the arc indicates a southeastward propagation (2.0 km/s eastward and 0.2 km/s equatorward). Following the eastward propagation of the arc, the shear layer (a vortical structure of the auroras rotating counterclockwise viewed antiparallel to the field lines) appeared at the western corner of Figure 6b. To highlight the auroras in the vortical structures and in the arcs, the dashed curves and lines are overlaid.

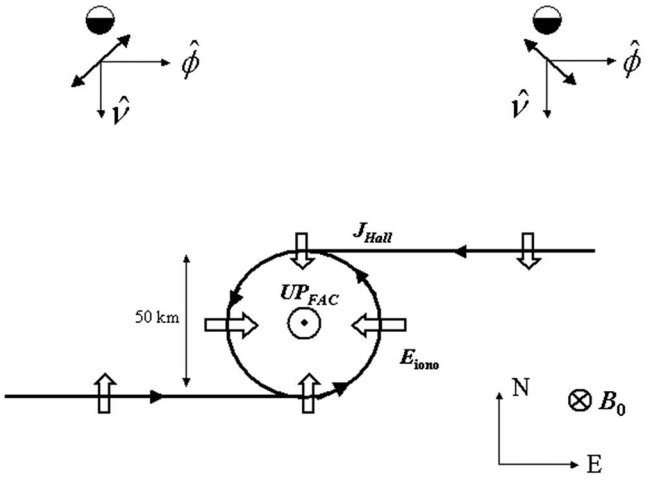

Figure 7. A schematic illustration summarizing the observation. (top right) Major axis orientation of the preonset waves at geosynchronous altitudes associated with southeastward propagating arc (before the passage of the shear layer). (top left) Same as in Figure 7 (top right) but for the southwestward propagating arc (after the passage of the shear layer). (bottom) Distribution of the ionospheric Hall currents (directed and loop currents, solid arrows) inferred from the auroral drifts and associated electric fields in open arrows (see text). The upward field-aligned currents associated with the divergence of the Pedersen currents are plotted at the center of the loop. The upward field-aligned currents are also associated with the auroral drift. The dimension of the loop is on the order of 50 km in the ionosphere. Note that the equatorward drift of the current system is neglected or viewed in the frame of the southward drift. The eastward drift of the loop is not included in the figure.

The shear layer moved eastward consecutively as shown by the overlaid dashed curves in Figures 6c–6e. The velocity of the head of the shear layer was 2.0 km/s eastward. The dashed lines in Figures 6b and 6c represent an auroral arc propagating eastward at latitudes poleward of the shear layer. The shear layer accompanied the auroral arcs at the equatorward latitudes as shown in Figures 6e and 6f. To view the motion of the auroras described above, auroral movies sampled at ~10 s from 04:30:00 UT to 04:55:00 UT are presented in Animation S1 in the supporting information. In the animation, the gray level image shows the brighter part of the auroras in white, viewed antiparallel to the field lines. East is to the left, and west is to the right in the animation.

2.3. Summary of the Observations

It is known that the equatorial continuity equation for flux tubes states that the flux tube content ($nv : v = \int ds/B$) in the frame of reference of the electric field drift are conserved if particle divergence arising from diamagnetic drift across the magnetic shell is neglected [*Lyons et al.*, 2003]. Assuming that the auroral luminosities were primarily related to the precipitating particles within the flux tube content, the continuity equation infers that the motion of auroras follows the electric field drift of flux tube in the equatorial plane. We interpret the auroral arc as the drift trajectories of the flux tube content, where particle density and the field magnitudes are higher than the surroundings. The higher-density increase precipitating flux and the increased field magnitudes enhance the flux loss by lowering the mirror height. The trajectories of these flux tube were mapped on the ionosphere as the auroral arc. The drift trajectories of the arc are also an auroral manifestation of the wavefront of the high-*m* Alfvén waves propagating equatorward [*Saka et al.*, 2014]. We assumed that the electric fields in the wavefront drive the ionospheric currents as a partial reflection of the high-*m* Alfvén waves at the earthward boundary [i.e., *Forget et al.*, 1991]. Figure 7 depicts these electric fields and associated Hall currents, where the equatorward drift of the wavefront is neglected or viewed in the frame of the equatorward drift.

Three types of currents were inferred: (1) loop currents at the center meridian, (2) westward currents associated with the eastward drift of the arc in the eastern sector, and (3) eastward currents associated with the westward drift of the arc in the western sector. The loop currents merged into the westward currents in the eastern sector and combined with the eastward currents in the western sector. The loop currents smoothed the "current discontinuity." The loop currents closing counterclockwise and the shear layer rotating clockwise (viewed from above the ionosphere) may accompany the converging electric fields. The northward and southward electric fields beside the loop are for the east-west motion of the arcs. Although the auroral drift associated with the shear layer did not complete the circle (see Figure 6d), the ionospheric current is assumed to form a loop. The converging electric fields in the ionosphere accompany the upward field-aligned currents in the center by the divergence of the Pedersen currents and the downward field-aligned currents in the surroundings to balance the total currents along the field lines. The orientations of the major axis observed at the geosynchronous altitudes are illustrated in the upper part of the figure. The orientation of the major axis is correlated with the current directions in the arc.

3. Theoretical Interpretation of the Observations

The equatorward expansion of the east-west aligned auroral arc is a signature observed in the auroral oval in the nightside sector. The equatorward drift of the arc progressed with intermittent intensifications and an east-west velocity component [*de la Beaujardiere et al.*, 1994]. These phenomena are associated with an increase in the transport of plasma sheet plasma across the boundary between open and closed magnetic field lines [*de la Beaujardiere et al.*, 1994]. The present case study revealed that the auroral arc accompanied the flow reversal at the meridian where the east-west velocity component was disconnected. The currents in the velocity discontinuity were joined by the loop current (see Figure 7).

The rotation of the major axis of the ULF oscillations was observed in the time interval when GOES 6 crossed the region magnetically conjugate to the current discontinuity in the ionosphere. This can be explained by assuming that the observed ULF waves are Alfvén waves with large azimuthal wave numbers ($m \gg 1$). The generation mechanism and spatial structure of such waves are fundamentally different from waves with small azimuthal wave numbers (m~1). The latter can be excited by the field line resonance (FLR) mechanism on resonance magnetic shells. Fast magnetosonic (FMS) waves that penetrate into the magnetosphere from the solar wind, or are generated on the plasmapause by the Kelvin-Helmholtz Instability, can serve as a source of these resonant Alfvén waves with m~1 (*Chen and Hasegawa*, 1974; *Southwood*, 1974). The Alfvén waves are excited by a FMS monochromatic wave on resonance magnetic shells, where their frequency ω coincides with the local frequency of Alfvén waves $\omega = k_0 v_A$.

In contrast to waves with m~1, azimuthally small-scale Alfvén waves cannot be excited by the FLR mechanism. FMS waves with $m \gg 1$ do not penetrate into the magnetosphere and cannot propagate inside it [*Leonovich and Mazur*, 2000]. Therefore, the source of the Alfvén waves with $m \gg 1$ has to be located on the same resonant magnetic shells where they are excited. In *Leonovich and Mazur* [1993], the external currents in the ionosphere were proposed as such a source. In particular, the variation of field-aligned currents flowing in and out of the ionosphere in the auroral zone can serve as a source. Of course, these currents can also excite magnetosonic waves. However, since for FMS oscillations with $m \gg 1$ the magnetosphere is the opacity region, they cannot be observed far from the ionosphere by the GOES 6 satellite [*Leonovich and Mazur*, 2000]. The same can be said about the slow magnetosonic (SMS) waves. SMS waves are strongly damped due to their interaction with the background plasma ions, and therefore, they cannot reach (with a sufficient amplitude) the GOES 6 orbit region [*Leonovich and Kozlov*, 2013]. Therefore, the only MHD oscillation mode with $m \gg 1$ excited in the ionosphere and observable by the satellites at magnetic field line tops is Alfvén waves.

To describe the structure of Alfvén waves in the magnetosphere, we use a curvilinear coordinate system (x^1, x^2, and x^3) tied to the geomagnetic field lines. The x^3 coordinate is directed along the field line, x^1 across magnetic shells, and x^2 in the azimuthal direction in which the plasma and the magnetic field are assumed to be uniform (see Figure 8). The same figure shows the spatial structure of a typical monochromatic standing Alfvén wave with $m \gg 1$, which can be represented as

$$b_\phi = U_N(x^1) H_N(x^1, x^3) e^{ik_2 x^2 - i\omega t},$$

where b_ϕ is the radial component of the oscillation magnetic field; $N = 1,2,3\ldots$ is the longitudinal wave numbering the harmonics of standing Alfvén waves; the $U_N(x^1)$ function describes the structure of the small-scale oscillations across magnetic shells; $H_N(x^1,x^3)$ describes the large-scale structure of standing Alfvén waves along magnetic field lines (Figure 8 shows the structure of the first harmonic $N = 1$); k_2 is the azimuthal wave number (if azimuthal angle ϕ is used as the x^2 coordinate, then $m = 0,1,2,3\ldots$ is the azimuthal wave number); and ω is the wave frequency. The $U_N(x^1)$ function is proportional to the intensity of field-aligned currents at the ionosphere level ($U_N(x^1) \sim j_{//}$). It describes a wave traveling between the two resonant surfaces—the poloidal (where the source frequency ω coincides with the local frequency of the Nth harmonic of standing poloidal Alfvén waves) and the toroidal (where ω coincides with the local frequency of the Nth harmonic of standing toroidal Alfvén waves). Field-aligned currents generate a poloidal standing Alfvén wave at the poloidal resonance surface, which then runs across magnetic shells to the toroidal surface, where finally, the waves are completely absorbed due to dissipation of their energy in the ionospheric conductive layer (see Figure 8). These Alfvén waves remain standing waves in the direction along the magnetic field lines. In the process, the poloidal standing wave is gradually transformed into a toroidal wave.

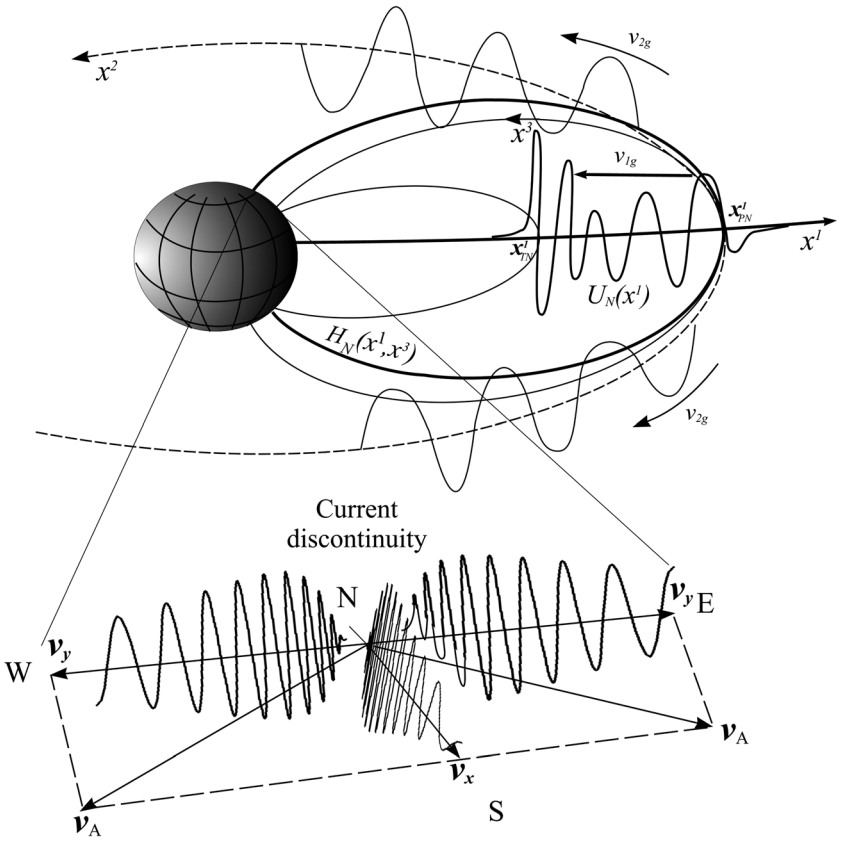

Figure 8. Schematic structure and propagation of the azimuthally small-scale Alfvén wave across the geomagnetic field lines in the magnetosphere and in projection on the ionosphere. The wave propagated away from the current discontinuity. N is for north, S is for south, W is for west, and E is for east.

Of course, external currents in the ionosphere generate a whole range of resonant Alfvén waves. However, some typical features of monochromatic oscillations persist for oscillations generated by a broadband source. Since all of the monochromatic oscillations represent waves propagating in the direction transverse to magnetic field lines, then the oscillation field they form is also a wave running in this direction. In particular, this wave has a group velocity across magnetic shells, v_{1g}, directed from the poloidal to toroidal resonance surface, which, when projected onto the ionosphere, results in waves propagating from the pole to the equator at velocity v_x (see Figure 8). Similarly, a wave moving in the azimuthal direction at velocity v_{2g} causes the perturbation to travel through the ionosphere at velocity v_y.

Let us now see how the oscillation polarization should change when the satellite intersects the current discontinuity. As it follows from div $\mathbf{b} = 0$, the relation in the transverse magnetic field components of the Alfvén waves is expressed as

$$b_\phi = \frac{i}{k_a}\nabla_r b_\theta, \tag{3}$$

where $k_a = m/\rho$ is the azimuthal component of the wave vector (ρ is the radius of point on a field line measured from the Earth's dipole field axis), ∇_r is the radial (across the magnetic shells) derivative, b_φ is the toroidal component, and b_θ is the poloidal component. The interaction of these waves with magnetospheric high-energy particles may lead to particle precipitations in the ionosphere and corresponding dynamics of the auroral arcs [*Leonovich et al.*, 2008]. Of course, the reason for auroral arc glow may not be related to Alfvén waves, but the similarity between the two dynamics indicates that this possibility exists.

Wave propagation across magnetic shells between the poloidal and toroidal resonance surfaces is mapped in their equatorward (or poleward) propagation with v_x velocity. Propagation in the azimuthal direction occurs with v_y velocity. On both sides of the current discontinuity, the wave propagation direction is oppositely

directed (the v_y signs are opposed), and thus, the azimuthal k_a component signs are also opposed. The $\nabla_r b_\theta$ sign does not change. As follows from equation (3), the b_ϕ sign does change. Therefore, when GOES 6 crossed the current discontinuity meridian, the inclination angle of the polarization ellipse changed, as shown in Figure 5. This also explains the gap in the keogram in the current discontinuity region, where field-aligned currents that are the source of the Alfvén waves had a rather small amplitude.

4. Discussion and Summary

It is conceivable that the ionospheric loop currents and field-aligned currents associated with the current discontinuity can excite standing high-*m* Alfvén waves in the magnetosphere [*Leonovich et al.*, 2008]. These Alfvén waves propagating away from the current discontinuity, equatorward and in the east-west directions (see Figure 8), were observed as ULF oscillations at geosynchronous altitudes. The currents excited the multiple high-*m* Alfvén waves; one was in the higher-frequency range in the 20–40 mHz band and the other in the lower frequencies in the 5 mHz band. The former waves decreased the activities while the loop propagated eastward across the GOES 6 meridian, while the activities of the latter waves remained throughout the west to east motion of the loop. The ULF frequencies of 30 mHz and 5 mHz and drift of the arc in an azimuthal direction (~2.0 km/s at the ionospheric altitudes) give the wave number m~260 and m~43, respectively.

The main results are summarized as follows:

1. Auroras with an east-west velocity discontinuity were observed in the equatorward drifting auroral arc.
2. The ionospheric loop currents are generated to connect the velocity discontinuities in the arc.
3. Field-aligned currents associated with the loop currents generated the high-*m* Alfvén waves in the magnetosphere.

Acknowledgments
The magnetometer data and the all-sky images used in the present study are from the Global Aurora Dynamics Campaign, STEP Polar Network (http://step-p.dyndns.org/~khay/). We thank both reviewers for their encouragements and fruitful comments. A.S. Leonovich thanks the Russian Scientific Foundation for supporting this work (section 3) by grant project 14-37-00027.

Michael Liemohn thanks the reviewers for their assistance in evaluating this paper.

References

Chen, L., and A. Hasegawa (1974), A theory of long-period magnetic pulsations: 1. Steady state excitation of field line resonance, *J. Geophys. Res.*, *79*, 1024–1032, doi:10.1029/JA079i007p01024.

de la Beaujardiere, O., L. R. Lyons, J. M. Ruohoniemi, E. Fris-Christensen, C. Danielsen, F. J. Rich, and P. T. Newell (1994), Quiet time intensifications along the poleward auroral boundary near midnight, *J. Geophys. Res.*, *99*, 287–298, doi:10.1029/93JA01947.

Forget, B., J.-C. Cerisier, A. Berthelier, and J.-J. Berthelier (1991), Ionospheric closure of small-scale Birkeland currents, *J. Geophys. Res.*, *96*, 1843–1847, doi:10.1029/90JA02376.

Glassmeier, K.-H., S. Buchert, U. Motschmann, A. Korth, and A. Pedersen (1999), Concerning the generation of geomagnetic giant pulsations by drift-bounce ring current instabilities, *Ann. Geophys.*, *17*(3), 338–350.

Hameiri, E., P. Laurence, and M. Mond (1991), The ballooning instability in space plasmas, *J. Geophys. Res.*, *96*, 1513–1526, doi:10.1029/90JA02100.

Karpman, V. I., B. I. Meerson, A. B. Mikhailovsky, and O. A. Pokhotelov (1977), The effects of bounce resonances on wave growth rates in the magnetosphere, *Planet. Space Sci.*, *25*(6), 573–585.

Klimushkin, D. Y., P. N. Mager, and V. A. Pilipenko (2012), On the ballooning instability of the coupled Alfvén and drift compressional modes, *Earth Planets Space*, *64*, 777–781, doi:10.5047/eps.2012.04.002, 2012.

Kozlov, D. A., A. S. Leonovich, and J. B. Cao (2006), The structure of standing Alfvén waves in a dipole magnetosphere with moving plasma, *Ann. Geophys.*, *24*, 263–274.

Leonovich, A. S., and D. A. Kozlov (2013), Magnetosonic resonances in the magnetospheric plasma, *Earth Planets Space*, *65*, 369–384.

Leonovich, A. S., and V. A. Mazur (1990), The spatial structure of poloidal Alfvén oscillations of an axisymmetric magnetosphere, *Planet. Space Sci.*, *38*(10), 1231–1241.

Leonovich, A. S., and V. A. Mazur (1993), A theory of transverse small-scale standing Alfvén waves in an axially symmetric magnetosphere, *Planet. Space Sci.*, *41*(9), 697–717.

Leonovich, A. S., and V. A. Mazur (2000), Structure of magnetosonic eigenoscillations of an axisymmetric magnetosphere, *J. Geophys. Res.*, *105*(A12), 27,707–27,716, doi:10.1029/2000JA900108.

Leonovich, A. S., D. A. Kozlov, and J. B. Cao (2008), Standing Alfvén waves with $m \gg 1$ in a dipole magnetosphere with moving plasma and aurorae, *Adv. Space Res.*, *42*, 970–978.

Lyons, L. R., C.-P. Wang, and T. Nagai (2003), Substorm onset by plasma sheet divergence, *J. Geophys. Res.*, *108*(A12), 1427, doi:10.1029/2003JA010178.

Mager, P. N., and D. Y. Klimushkin (2008), Alfvén ship waves: High-*m* ULF pulsations in the magnetosphere generated by a moving plasma inhomogeneity, *Ann. Geophys.*, *26*, 1653–1663.

Radoski, H. (1974), A theory of latitude dependent geomagnetic micropulsations: The asymptotic fields, *J. Geophys. Res.*, *79*, 595–603, doi:10.1029/JA079i004p00595.

Saka, O., D. Koga, and K. Hayashi (2007), A plasma bulk motion in the midnight magnetosphere during auroral breakup inferred from all-sky image and magnetic field observations at geosynchronous altitudes, *J. Atmos. Sol. Terr. Phys.*, *69*, 1063–1074.

Saka, O., K. Hayashi, and M. Thomsen (2010), First 10 min intervals of Pi2 onset at geosynchronous altitudes during the expansion of energetic ion regions in the nighttime sector, *J. Atmos. Sol. Terr. Phys.*, *72*, 1100–1109.

Saka, O., K. Hayashi, and M. Thomsen (2014), Preonset auroral signatures and subsequent development of substorm auroras: A development of ionospheric loop currents at the onset latitudes, *Ann. Geophys.*, *32*, 1011–1023.

Southwood, D. J. (1974), Some features of field line resonances in the magnetosphere, *Planet. Space Sci.*, *22*, 483–491.